Examination of Spinel and Nonspinel Structural Models for γ-Al_2O_3 by DFT and Rietveld Refinement Simulations

Mingyong Sun,[†] Alan E. Nelson,*[,†] and John Adjaye[‡]

Department of Chemical and Materials Engineering, University of Alberta, Edmonton, Alberta, Canada T6G 2G6, and Edmonton Research Centre, Syncrude Canada Ltd., Edmonton, Alberta, Canada T6N1H4

Received: November 8, 2005

Despite the widespread use of γ-Al_2O_3, there is still considerable disagreement over the nature of its structure due to both its poor crystallinity and differing preparation techniques during experimentation. Using density-functional theory (DFT) calculations and Rietveld simulations and refinement, the structure of three spinel-related models and a recently proposed nonspinel model were studied in reference to synchrotron X-ray powder diffraction (SXPD) patterns. The spinel-based structural models represent the structural features of γ-Al_2O_3 better than the nonspinel model. The major failure of the nonspinel model is that the model cannot reproduce the SXPD reflection originating from tetrahedral aluminum. The Rietveld-refined spinel model can accurately reproduce the lattice parameters and other structural features of γ-Al_2O_3, and it can generate a consistent diffraction peak at 2θ which lies between the splitting peaks of the experimental pattern that are originated from the disordered tetrahedral aluminum cations.

1. Introduction

Due to the widespread application of γ-alumina (γ-Al_2O_3), specifically in the petroleum and petrochemical industries as a catalyst and/or catalyst support,[1,2] understanding the surface properties of γ-Al_2O_3 and the interaction between the active components and the support is critical to elucidate the structure−property relationship of this industrially significant material. γ-Al_2O_3 has traditionally been described as having a defective spinel structure,[3−6] whereby mineral spinel $MgAl_2O_4$ is the parent compound of the spinel structural models. The cubic unit cell of a spinel structure possesses a face centered cubic (fcc) sublattice of oxygen ions. There are 96 interstices between the oxygen ions in the cubic cell; 64 are tetrahedral (8a, 8b, and 48f), and 32 are octahedral (16c and 16d). In spinel $MgAl_2O_4$, magnesium ions occupy tetrahedral 8a positions and aluminum ions 16d positions,[3] and these cation positions are referred to as spinel sites.[6] Due to the difference in the cation-to-oxygen ratio between Al_2O_3 and $MgAl_2O_4$ (2−3 vs 3−4), the spinel structure of Al_2O_3 includes vacancies at cation positions to accommodate the stoichiometric requirement. Many studies have contributed to resolving the distribution of cation vacancies in the defect spinel structure of γ-Al_2O_3, and differing conclusions have been made.[6−11] Some experimental observations support that cation vacancies are primarily located at octahedral sites,[7,9] while other studies favor the opposite conclusion.[8,10,11] In a recent DFT study, Wolverton and Hass found that cation vacancies energetically preferred octahedral sites.[6]

The existence of hydrogen in the bulk structure and its distribution have also been the subject of studies regarding the detailed structure γ-Al_2O_3.[6,12−14] It is widely accepted that there are hydroxyl groups on the surface of γ-Al_2O_3, but opinions about the existence of hydrogen in the bulk structure of γ-Al_2O_3 have not reached a consensus in the literature. Pearson studied the distribution of protons between surface and bulk phases of transition aluminas and reported that about 0.0033 g of H/g alumina was present in the bulk phase of alumina.[14] On the basis of weight loss of γ-Al_2O_3 upon thermal treatment, Soled[15] and Zhou and Snyder[13] also reported that hydrogen was present in the bulk phase of γ-Al_2O_3. Tsyganenko et al. found that the −OH vibrational bands (ν_{OH}) at about 3500 and 3300 cm^{-1} are not affected by CO or pyridine adsorption or D_2O treatment at low temperature, which further supports the existence of hydrogen in the bulk phase of γ-Al_2O_3.[16] On the basis of small-angle X-ray scattering (SAXS) and prompt-γ activation analysis, Paglia et al. reported that hydrogen-containing species other than water were present in the bulk structure of γ-Al_2O_3; however, they suggested that hydrogen was not at interstitial positions and limited to the surface or within the amorphous content of the material.[17] On the basis of DFT calculations, Sohlberg et al. supported the presence of various amounts of hydrogen within the bulk structure of spinel γ-Al_2O_3,[12] while Wolverton and Hass indicated that hydrogen spinel (HAl_5O_8) is thermodynamically unstable with respect to decomposition into an anhydrous defect spinel plus boehmite.[6]

Within the framework of the spinel structural model, several studies reported that it is possible that aluminum cations are located at oxygen interstices other than spinel sites.[18] Zhao and Snyder suggested that 75% of aluminum atoms occupy spinel sites, of which 43% are at 16d and 32% at 8a, and the other 25% of quasi-octahedral aluminum occupy the 32e sites, which are only 0.372 Å from the octahedral 16c sites.[13] Recently, a complete nonspinel structure was proposed based on molecular dynamic simulations and DFT calculations of the dehydration of boehmite.[19,20] In this nonspinel structural model, γ-Al_2O_3 still possesses an fcc sublattice of oxygen atoms that form octahedral and tetrahedral interstices, in which aluminum atoms are located.[20] The most stable structure of the nonspinel model

* To whom correspondence should be addressed. Tel: +1-780-492-7380. Fax: +1-780-492-2881. E-mail: alan.nelson@ualberta.ca.
[†] University of Alberta.
[‡] Syncrude Canada Ltd.

10.1021/jp056465z CCC: $33.50
Published on Web 01/13/2006

contains 25% tetrahedral aluminum, and its detailed crystallographic structure has been provided in ref 20. This nonspinel model showed good agreement with some experimental data in terms of structural parameters, percentage of aluminum atoms in tetrahedral sites, and a simulated XRD pattern.[20] However, direct comparison between the spinel-related models and the nonspinel model is needed to facilitate a better assessment of proposed models for the structure of γ-Al_2O_3.

In the present study, we have performed detailed DFT calculations for different spinel-related γ-Al_2O_3 structures combined with Rietveld refinement analysis and compared them with the nonspinel structural model in order to provide additional insights into the structure of γ-Al_2O_3. The correct structural model should be able to represent the known structural properties observed by different experimental techniques, including the composition and relative stability of different structures. The percentage of aluminum in γ-Al_2O_3 that has a tetrahedral coordination determined by solid-state NMR is always reported in the range of 21−31%.[8,11,21] Thus, in this study, each of the proposed models is initially analyzed to verify they can predict a percentage of tetrahedral aluminum within this compositional range. Then, the relative stability of each model is compared based on relative energies obtained by plane-wave DFT calculations. The structural models are further assessed by comparing their simulated diffraction patterns against an experimental synchrotron X-ray powder diffraction (SXPD) pattern for a commercial γ-Al_2O_3 sample (Davicat AL2700). Qualitative examination of the simulated diffraction patterns against the experimental pattern and quantitative evaluation based on the profile factor (R_p) are used to assess the quality of the models.

2. Experimental and Modeling

2.1. DFT Calculations. Density-functional theory (DFT) calculations were performed using Material Studio CASTEP from Accelrys (version 3.2) based on a plane-wave pseudopotential method.[22] Ultrasoft pseudopotentials are used to describe ion−electron interactions.[23] The cutoff energy for the plane-wave basis set is set at 310 eV, with a k-point separation at 0.05 $Å^{-1}$. The GGA-PBE nonlocal gradient-corrected exchange functional is used to describe the exchange-correlation energy and potential.[24] The convergence criterion for the SCF cycle is set at 2×10^{-7} eV/atom. The geometry optimization (atom relaxation) convergence thresholds for energy change, maximum force, and maximum displacement between optimization cycles are 2×10^{-5} eV/atom, 0.05 eV/Å, and 0.002 Å, respectively. The cell parameters for each model are also optimized during geometry optimizations.

2.2. Powder Diffraction Simulation and Refinement. The powder diffraction patterns of all models discussed in this work are calculated and refined against experimental data using the Reflex Plus module from Accelrys. The powder refinement is performed using Rietveld analysis implemented in the Reflex Powder Refinement tool based on standard algorithms employed in Rietveld refinement.[25,26] The quality of the fit between the simulated and experimental data is expressed by the profile *R*-factor, R_p

$$R_p = \frac{\sum_i |cY^{sim}(2\theta_i) - I^{exp}(2\theta_i) + Y^{back}(2\theta_i)|}{\sum_i |I^{exp}(2\theta_i)|} \quad (1)$$

where c is a constant scaling factor optimized to obtain the lowest value of R_p, $Y^{sim}(2\theta_i)$ is the simulated diffraction intensity without the background contribution, $I^{exp}(2\theta_i)$ is the measured experimental spectrum, and $Y^{back}(2\theta_i)$ is the background intensity of the measured spectrum.

TABLE 1: Comparison of Calculated and Experimental Structure Parameters of α-Alumina

lattice parameters	DFT calculated	Rietveld refined	experimental
a, Å	4.718	4.7552 ± 0.0007	4.7628
b, Å	4.718	4.7612 ± 0.0006	4.7628
c, Å	12.903	13.009 ± 0.001	13.003
α, deg	90.00	89.99 ± 0.01	90
β, deg	90.00	89.91 ± 0.02	90
γ, deg	120.00	119.87 ± 0.01	120

2.3. Synchrotron Powder Diffraction. A high-resolution powder diffraction spectrum of a commercial γ-Al_2O_3 sample (Davicat AL2700) was recorded at the X3B1 beamline at the National Synchrotron Light Source (NSLS) at Brookhaven National Laboratory (BNL). The X3B1 synchrotron beam is monochromated by a double Si(111) crystal monochromator at a wavelength of 0.69876 Å, as calibrated from a series of seven well-defined reflections using a NIST corundum X-ray diffraction standard (NIST 1976a). The intensity of the incident beam was monitored by an ion chamber and normalized for the decay of the primary beam, and the diffracted beam was analyzed with a Ge(111) crystal. X-ray scattering intensities were collected at room temperature using a nominal 1.5 mm capillary in steps of 0.01° by counting for 6 s at every 2θ from 5° to 75°. It should be noted that the resolution of the diffractometer is much higher than the peaks observed from the γ-Al_2O_3 sample.

3. Results and Discussion

3.1. Modeling α-Alumina Structure. To verify the present methodology, DFT calculations and Rietveld analysis were initially applied to study the structure of α-alumina, which possesses a well-defined and characterized structure.[27] The structure of α-alumina was first geometrically optimized, including lattice parameters and atom coordination, to determine the detailed structure with minimum electronic energy (energy minimization) using DFT plane-wave calculations (GGA-PBE). The structure was subsequently refined against an experimental XRD pattern of a commercial α-alumina (from Alfa Aesar) using Rietveld refinement. The DFT calculated and Rietveld-refined structural parameters are listed in Table 1. The experimental data from ref 27 are also listed in Table 1 for comparison.

The results indicate that the DFT structural optimization underestimates the lattice constant by ≤1% relative to the experimental data. In addition to GGA-PBE, other exchange-correlation functionals, including GGA-PW91 and GGA-RPBE, were also checked and similar levels of accuracy were obtained; each functional produced lattice constants with less than 1% error relative to the experimental data. Previous plane-wave DFT calculations with GGA-PW91 using different simulation software also obtained a similar level of accuracy for α-alumina lattice parameters.[6] However, an earlier DFT calculation underestimated the lattice constants of α-alumina by about 6%.[12] The DFT calculations performed in the present study are highly accurate and comparable with other state-of-the-art calculations.

An experimental XRD pattern (Cu Kα radiation with a graphite monochromator) for the commercial α-alumina sample (Alfa Aesar) was collected, and the optimized α-alumina structural model structure was further refined using Rietveld refinement against the experimental XRD pattern. The results listed in Table 1 clearly show that the refined parameters are nearly identical to the experimental parameters. Within a

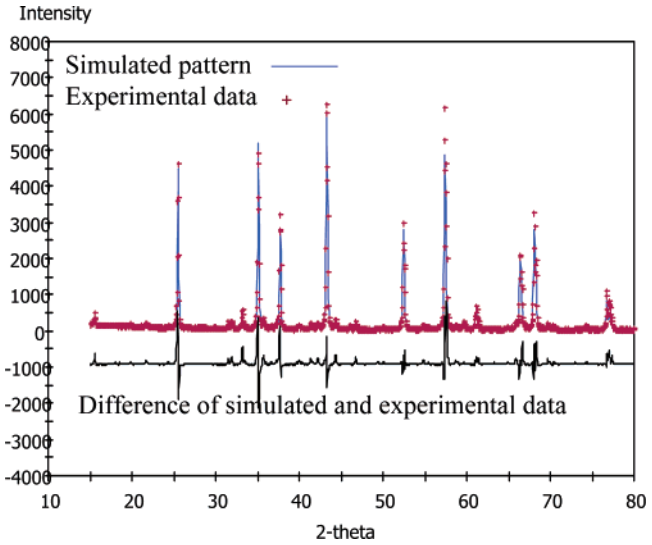

Figure 1. Simulated diffraction pattern of α-alumina against experimental XRD data.

tolerance of 0.1 Å, the Rietveld-refined structure still maintains the hexagonal symmetry with the parameters being $a = b = 4.7614$ Å. Figure 1 presents the simulated and experimental XRD patterns of α-alumina, and an excellent agreement is qualitatively evidenced and quantitatively supported by an R_p value of 21.96%.

From these results, it can be concluded that the plane-wave DFT geometrical optimization calculations can produce lattice parameters within 1% accuracy and that Rietveld refinement can further modify the structure to obtain accurate lattice parameters with errors less than 0.01 Å. In the present study, this approach was subsequently used to assess all possible models derived from the spinel structure and compare them with the nonspinel structure model in reference to experimentally observed data.

3.2. Spinel-Related γ-Alumina Structural Models. 3.2.1. Fully and Partly Hydrogenated Structure. As mentioned in the Introduction, the cubic unit cell of spinel $MgAl_2O_4$ includes 32 oxygen atoms in the Wyckoff 32e positions, 16 aluminum atoms in the 16d positions, and 8 magnesium atoms in the 8a positions.[3] When every two magnesium cations in the cubic $MgAl_2O_4$ structure are replaced by a proton and an aluminum cation, the fully hydrogenated γ-Al_2O_3 model is generated with a formula $H_4Al_{20}O_{32}$. The structure with protons located at perfect spinel cation positions, where hydrogen atoms are not bonded to oxygen, is only a local minimum; protons are more stable when they are bonded to neighboring oxygen atoms to form bulk −OH groups. The protons can be located entirely at either tetrahedral or octahedral locations or between these two types of positions with one, two, or three protons in tetrahedral positions. Thus, five possible models can be generated, namely, $H^T{}_4Al^T{}_4Al^O{}_{16}O_{32}$, $H^O{}_4Al^T{}_8Al^O{}_{12}O_{32}$, $H^T{}_3H^OAl^T{}_5Al^O{}_{15}O_{32}$, $H^T{}_2H^O{}_2Al^T{}_6Al^O{}_{14}O_{32}$, and $H^TH^O{}_3Al^T{}_7Al^O{}_{13}O_{32}$. In these structural formulas, the superscript O indicates the octahedral position and T the tetrahedral position.

The γ-Al_2O_3 structures were fully optimized by DFT calculations, and their energies relative to α-alumina and free water expressed as per Al_2O_3 are listed in Table 2. Since all these structures have the same number of atoms, their relative energies can directly indicate which structure is more stable than the others, regardless of what structural state is taken as the reference. The model with protons only occupying the tetrahedral positions ($H^T{}_4Al^T{}_4Al^O{}_{16}O_{32}$) produces a structure with 0.13 eV/Al_2O_3 higher energy than that with protons at octahedral locations ($H^O{}_4Al^T{}_8Al^O{}_{12}O_{32}$). Using a smaller supercell containing 42 atoms ($H_3Al_{15}O_{24}$), Wolverton and Hass also predicted that protons slightly prefer octahedral locations but only by 0.005 eV/Al_2O_3.[6] The larger supercell, allowing more freedom during geometry optimization, magnifies the difference between these two structures. In the structure of $H^O{}_4Al^T{}_8Al^O{}_{12}O_{32}$, 40% of aluminum cations are at the tetrahedral positions, which is much higher than the experimentally observed data. Therefore, several additional possible distributions of protons in the bulk structure were examined, and it was found that the model with protons evenly distributed between tetrahedral and octahedral positions ($H^T{}_2H^O{}_2Al^T{}_6Al^O{}_{14}O_{32}$) yields the structure with the lowest relative energy. This structure predicts a relative tetrahedral aluminum concentration of 30% (Table 2), which is within the range (21−31%) observed experimentally by NMR.[8,11,21]

TABLE 2: Summary of Different Models for γ-Alumina

model	relative energy[a], eV/Al_2O_3	Al^T, %	R_p, %
Fully Hydrogenated			
$H^T{}_4\ Al^T{}_4Al^O{}_{16}O_{32}$	0.20	20.0	13.2
$H^O{}_4\ Al^T{}_8Al^O{}_{12}O_{32}$	0.07	40.0	14.2
$H^T{}_3\ H^OAl^T{}_5Al^O{}_{15}O_{32}$	0.14	25.0	12.0
$H^T{}_2\ H^O{}_2\ Al^T{}_6Al^O{}_{14}O_{32}$	0.04	30.0	11.7
$H^TH^O{}_3\ Al^T{}_7Al^O{}_{13}O_{32}$	0.12	35.0	12.0
Partly Hydrogenated			
$H^T□^O□^TAl^T{}_6Al^O{}_{15}O_{32}$	0.14	28.6	12.5
$H^T□^T{}_2Al^T{}_5Al^O{}_{16}O_{32}$	0.34	23.8	12.8
$H^O□^O□^TAl^T{}_7Al^O{}_{14}O_{32}$	0.18	33.3	11.9
$H^O□^T{}_2Al^T{}_6Al^O{}_{15}O_{32}$	0.13	28.6	11.5
Defect Spinel			
$□^O{}_2Al^T{}_6Al^O{}_{10}O_{24}$	0.13	37.5	14.4
$□^O□^TAl^T{}_5Al^O{}_{11}O_{24}$	0.27	31.5	10.0
$□^T{}_2Al^T{}_4Al^O{}_{12}O_{24}$	0.39	25.0	11.8
Nonspinel model	0.20	25.0	13.6

[a] Relative energies of different types of structure models have used α-alumina and free H_2O as references to account for the atomic balance between models with different amounts of hydrogen.

X-ray diffraction patterns of the structural models were simulated without modifying the lattice parameters and compared with the experimental SXPD pattern of Davicat AL2700 using Rietveld refinement. The R_p factors are listed in Table 2. It is interesting to note that the model with lowest relative energy also has the smallest R_p factor. These results indicate that the protons have no strong preference to either tetrahedral or octahedral vacancies in the bulk γ-Al_2O_3 structure. When protons are distributed between octahedral and tetrahedral positions, the structure is energetically more stable, predicts reasonable percentage of tetrahedral aluminum, and produces a lower R_p value (Table 2).

If three protons are removed from the fully hydrogenated model and replaced by one aluminum cation, the spinel structure contains one proton and two cation vacancies; thus, a partly hydrogenated model can be generated (the second section in Table 2). The proton can be located at octahedral or tetrahedral positions, and the two vacancies can be both at tetrahedral positions or one at a tetrahedral location and one at an octahedral position. A model with both vacancies located at octahedral positions not only gives a too high percentage of tetrahedral aluminum but also produces the greatest error in reference to the experimental SXPD data. The model with a proton at a tetrahedral site and two vacancies distributed between octahedral and tetrahedral vacancies ($H^T□^O□^TAl^T{}_6Al^O{}_{15}O_{32}$) and the model with a proton at an octahedral site and two vacancies at the tetrahedral sites ($H^O□^T{}_2Al^T{}_6Al^O{}_{15}O_{32}$) are energetically more stable than the other two models. Additionally, both structural

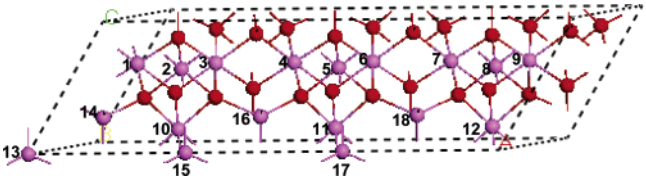

Figure 2. (3 × 1 × 1) supercell of $MgAl_2O_4$ including three primitive cells with Mg replaced by Al, and the aluminum atoms are numbered from 1 to 18.

TABLE 3: Vacancy Distribution and Relative Energy of the Defective Spinel Structure in Figure 2

vacancy positions	relative energy[a] eV/Al_2O_3	Al^T, %	vacancy positions	relative energy[a] eV/Al_2O_3	Al^T, %
1 and 2	0.60	37.5	1 and 12	0.61	37.5
1 and 3	0.60	37.5	1 and 13	0.27	31.3
1 and 4	0.25	37.5	1 and 14	0.27	31.3
1 and 5	0.14	37.5	1 and 15	0.27	31.3
1 and 6	0.13	37.5	1 and 16	0.28	31.3
1 and 7	0.25	37.5	1 and 17	0.28	31.3
1 and 8	0.61	37.5	1 and 18	0.28	31.3
1 and 9	0.60	37.5	3 and 7	0.13	37.5
1 and 10	0.60	37.5	14 and 18	0.57	25.0
1 and 11	0.14	37.5	15 and 18	0.39	25.0

[a] α-Alumina is used as the energy reference.

models predict a reasonable percentage of tetrahedral aluminum (28.6%), however, the $H^O\square^T{}_2Al^T{}_6Al^O{}_{15}O_{32}$ model has a lower R_p value of 11.5% (Table 2).

3.2.2. Dehydrogenated Defect Spinel Structure. A fully dehydrogenated γ-Al_2O_3 structure can be generated by replacing the proton in the partly hydrogenated structure by one-third of an aluminum cation and two-thirds vacancies to balance the charge, with a generated cubic unit cell formula of $\square_{2\ 2/3}Al_{21\ 1/3}O_{32}$. A fully dehydrogenated defect γ-Al_2O_3 model can be generated using a supercell including three primitive cells of $MgAl_2O_4$, with each primitive cell including eight oxygen atoms, four aluminum atoms, and two magnesium atoms to obtain a fully dehydrogenated structure model with integer numbers of atoms and vacancies. In the (3 × 1 × 1) supercell of $MgAl_2O_4$, the six Mg^{2+} are replaced by four Al^{3+} and two cation vacancies to create the dehydrogenated structural model with the formula $\square_2Al_{16}O_{24}$. The two vacancies within this structure can be created at different locations with various combinations of tetrahedral and octahedral positions, as illustrated in Figure 2. Aluminum cations numbered from 1 to 12 are at the octahedral positions, and those numbered from 13 to 18 are at the tetrahedral positions. Table 3 presents the relative energies of structures with vacancies being created at different locations.

From the relative energies, it can be concluded that on the basis of structural energetics the vacancies prefer to be located at octahedral positions and that the two vacancies prefer to be separated from each other. The energy range between the highest and lowest is 0.47 eV/Al_2O_3, and the lowest energy of the defect spinel structure is 0.13 eV/Al_2O_3 higher than that of α-alumina. This is in excellent agreement with the DFT-GGA calculation results of Wolverton and Hass.[6] The model with two vacancies occupying the octahedral positions, however, predicts too high of a tetrahedral aluminum percentage (37.5%) compared to relative experimental concentrations reported based on NMR measurements.[8,11,21] The models with one vacancy at one octahedral and one at the tetrahedral location have slightly higher energy (ΔE = 0.14 eV/Al_2O_3), and the predicted tetrahedral aluminum percentage (31.5%) is close to experimental results. When two vacancies occupy two separate tetrahedral positions, the relative energy of the structure increases by an additional 0.12 eV/Al_2O_3; this model predicts 25% tetrahedral aluminum, which is within the range of experimental data.

One structure with the lowest energy from each group, vacancies at two tetrahedral ($\square^T{}_2Al^T{}_4Al^O{}_{12}O_{24}$), one tetrahedral and one octahedral ($\square^O\square^TAl^T{}_5Al^O{}_{11}O_{24}$), and two octahedral ($\square^O{}_2Al^T{}_6Al^O{}_{10}O_{24}$) positions, was further analyzed to evaluate the model against the experimental SXPD pattern. The Rietveld refinement results (Table 2) indicate that the simulated SXPD pattern of the structural model with vacancies at both tetrahedral and octahedral positions ($\square^O\square^TAl^T{}_5Al^O{}_{11}O_{24}$) is closest to the experimental pattern (R_p = 10.0%); this model predicts 31.5% tetrahedral aluminum atoms.

As it was mentioned previously, there is a disagreement regarding the distribution of cation vacancies in the γ-Al_2O_3 bulk structure. The results in Table 2 show that for the fully dehydrogenated defect spinel model the structure with all vacancies at octahedral positions has the lowest energy, but this structure also produces the largest error with Rietveld refinement of experimental SXPD data (Table 2). As a transition alumina, γ-Al_2O_3 has a metastable nature; the most stable structure does not necessarily describe an actual γ-Al_2O_3 sample with the highest accuracy. Besides relative energetics, other properties, such as powder diffraction and NMR data, also need to be considered in the evaluation of possible models for γ-Al_2O_3. When all the cation vacancies are located at the octahedral sites, the structure predicts much more tetrahedral aluminum (37.5%) than that experimentally observed (21−31%). The large R_p value also disfavors the model with all vacancies located on the tetrahedral sites. Therefore, it can be concluded that aluminum atoms prefer tetrahedral locations with octahedral sites vacant to reduce the energy of the structure, but during the preparation of γ-Al_2O_3, some tetrahedral locations may also be vacant in addition to octahedral positions. Because γ-Al_2O_3 is a transition structure between boehmite and α-alumina through δ- and θ-alumina, the ratio of the two types of vacancies depends on the preparation conditions. The structure with vacancies evenly distributed between octahedral and tetrahedral sites has a mid-energy level and produces a simulated diffraction pattern which is in excellent agreement with experimental SXPD data (Table 2).

3.2.3. Thermodynamic Stability of the Hydrogenated Structures. The results presented in Table 2, taking α-alumina and free H_2O molecule as energy references, show that the lowest energy structure of fully hydrogenated model ($H^T{}_2H^O{}_2Al^T{}_6Al^O{}_{14}O_{32}$) is about 0.10 eV/$Al_2O_3$ lower than the lowest energy structure of anhydrous defect spinel model ($\square^O{}_2Al^T{}_6Al^O{}_{10}O_{24}$) and 0.23 eV/$Al_2O_3$ lower than the structure ($\square^O\square^TAl^T{}_5Al^O{}_{11}O_{24}$) with the lowest R_p value (Table 2). Removing the structural hydrogen from $H^T{}_2H^O{}_2Al^T{}_6Al^O{}_{14}O_{32}$ to $\square^O{}_2Al^T{}_6Al^O{}_{10}O_{24}$ in the form of gas-phase water is an endothermic process (ΔE = 0.5 eV/H_2O) which increases (ΔE = 1.2 eV/H_2O) if $\square^O\square^TAl^T{}_5Al^O{}_{11}O_{24}$ is considered as the dehydrated structure. Sohlberg et al.[12] also reported that the hydrogen spinel (HAl_5O_8) was lower in total energy than the anhydrous defect spinel when a free water molecule was used as a reference and concluded that hydrogen could exist in the bulk structure in the form of bulk −OH groups. Wolverton and Hass,[6] however, pointed out that hydrogen spinel is thermodynamically unstable if liquid H_2O instead of gas-phase H_2O was taken as energy reference.

Thus, more detailed thermodynamic analysis was performed to characterize the process of removing hydrogen from the fully

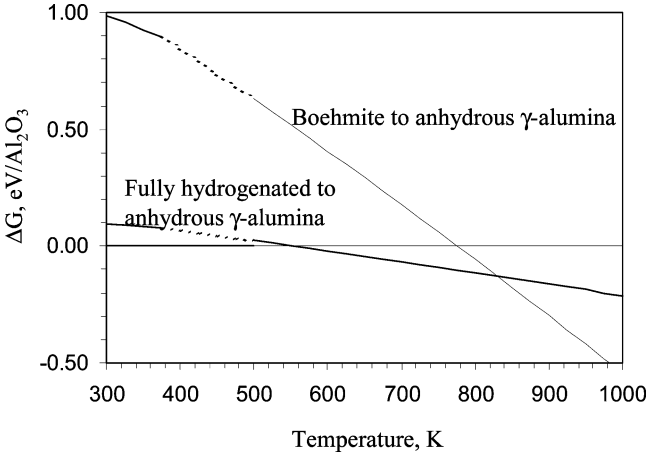

Figure 3. Free energy changes for the dehydration from fully hydrogenated γ-alumina and boehmite to anhydrous γ-alumina at 1 atm.

hydrogenated structure in the form of water. The process is described as

$$\frac{1}{10}(H_4Al_{20}O_{32}) = \frac{1}{8}(Al_{16}O_{24}) + \frac{1}{5}H_2O \quad (1)$$

($H_4Al_{20}O_{32}$) and ($Al_{16}O_{24}$) represent fully hydrogenated and anhydrous structures, respectively, with each side of the equation normalized to include one formula Al_2O_3. The relative stabilities of these structures are determined by the free energy change of the processes.

$$\Delta G_1 = \frac{1}{8}G_{Al_{16}O_{24}} + \frac{1}{5}G_{H_2O} - \frac{1}{10}G_{H_4Al_{20}O_{32}} \quad (2)$$

In eq 2, ΔG_1 is the free energy change for process (1), and $G_{H_4Al_{20}O_{32}}$, $G_{Al_{16}O_{24}}$, and G_{H_2O} are the free energies of the corresponding materials at the temperature of interest. For different structures of the solid phase, it is assumed their temperature dependence and entropic effect are similar and can be canceled in free energy change calculation. However, for water, the temperature effect and entropy contribution cannot be neglected. Thus, for the gas phase

$$G^{g,T}_{H_2O} = H^{g,T}_{H_2O} - TS^{g,T}_{H_2O} = E^{g,0K}_{H_2O} + (H^{g,T}_{H_2O} - E^{g,0K}_{H_2O}) - TS^{g,T}_{H_2O} \quad (3)$$

and for the liquid phase

$$G^{l,T}_{H_2O} = H^{l,T}_{H_2O} - TS^{l,T}_{H_2O} = E^{g,0K}_{H_2O} + (H^{g,T}_{H_2O} - E^{g,0K}_{H_2O}) - \Delta H^{vap}_{H_2O} - TS^{l,T}_{H_2O} \quad (4)$$

where $G^{g,T}_{H_2O}$ and $G^{l,T}_{H_2O}$ are the free energies of H_2O at temperature T in the gas phase and liquid phase, respectively. $E^{g,0K}_{H_2O}$ is the total energy of free H_2O molecule at 0 K, and ($H^{g,T}_{H_2O} - E^{g,0K}_{H_2O}$) is the temperature correction of enthalpy from 0 to T K for gas-phase H_2O, which can be obtained by ab initio DFT calculations of normal-mode frequencies including the zero-point vibrational energy. The entropy of gas-phase water, $S^{g,T}_{H_2O}$, at $T > 500$ K, and that of liquid-phase water, $S^{l,T}_{H_2O}$, at $T < 375$ K are experimental data from the NIST online database.[28] The gas-phase entropy was also calculated from the DFT normal-mode frequencies, and it was noted that the calculated values are the same as the experimental values for gas-phase water at $T > 500$ K. Figure 3 plots ΔG_1 against temperature, where at $T < 375$ K liquid-phase water is the reference and at $T > 375$ K gas-phase water is the reference. The data between 375 and 500 K are calculated values (dashed line) considering water behaves as an ideal gas. The smooth connection between the three regions indicates that the effect of nonideality of water in the gas phase below 500 K on entropy is insignificant.

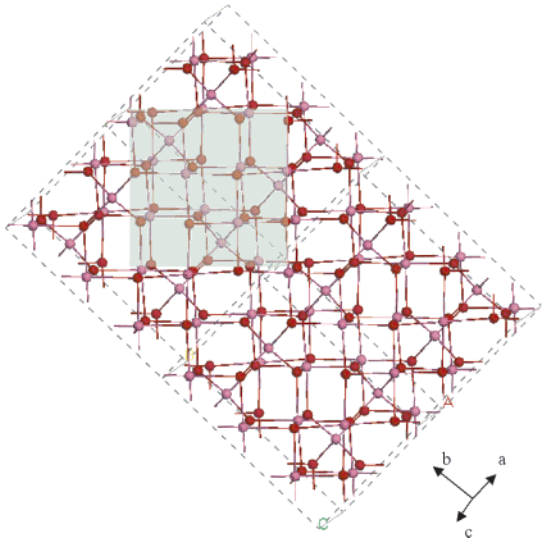

Figure 4. Nonspinel model constructed using the structural parameters reported in ref 20. The shaded area indicates the spinel orientation of the structure.

Figure 3 shows that the ΔG_1 values at $T < 550$ K are above zero, which indicates that the hydrogenated structure of γ-Al_2O_3 is more stable than the anhydrous structure at low temperatures. Only at elevated temperatures higher than 550 K is the anhydrous form of γ-Al_2O_3 more stable. This result is counter to the conclusion by Wolverton and Hass.[6] In their work, they neglected the temperature correction term for enthalpy from 0 K to T, ($H^{g,T}_{H_2O} - E^{g,0K}_{H_2O}$) and directly used the $E^{g,0K}_{H_2O}$ to represent the enthalpy at T (eq 5 in ref 6). This temperature correction term is significant compared with the entropy term, TS. For example, at 298 K (liquid phase), the temperature correction term is 0.66 eV/H_2O compared to 0.22 eV/H_2O for the entropy term (TS), and at 700 K (gas-phase), the temperature correction term is 0.81 eV/H_2O compared to 1.6 eV/H_2O for the entropy term (TS). Neglecting this term would result in a significant error in comparing the relative stability of different structures (about 0.6 and 0.9 eV/H_2O), which should be contrasted with the energy differences between the structures listed in Table 2, all of which are less than 0.3 eV/Al_2O_3, and the energy of boehmite relative to α-alumina and water, which is −0.87 eV/Al_2O_3.

In addition, the free energy change for the dehydration of boehmite to γ-alumina is also included in Figure 4. The ΔG for this process is positive until the temperature reaches 775 K, which is the minimum temperature required for transforming boehmite to γ-Al_2O_3. Krokidis et al. noted that the lowest temperature experimentally observed for the transformation of boehmite to transition alumina was approximately 100 K higher than they predicted by thermodynamic analysis.[19] In their thermodynamic analysis, they also neglected the temperature correction term for enthalpy (see eq 7 in ref 19). By adding this term, the predicted temperature required for the transformation to take place would be about 100 K higher, which would agree with the experimental result.

3.3. Nonspinel Model. Krokidis et al. proposed a complete nonspinel model based on molecular dynamic simulation and DFT calculations of the dehydration of boehmite.[19] The most

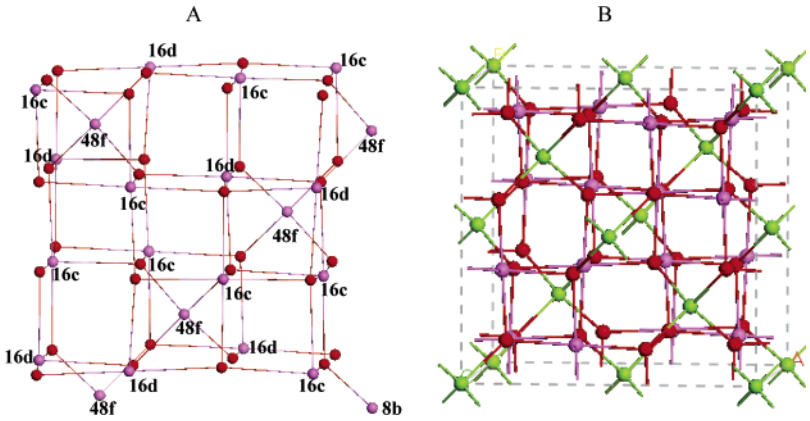

Figure 5. Comparison of the cation positions in the nonspinel structure (A) and in the spinel structure. The cation positions are labeled in the nonspinel structure (A); tetrahedral cations occupy 8a and octahedral 16d in the spinel structure.

stable structure of the nonspinel model contains 25% tetrahedral aluminum, and its detailed crystallographic structure has been provided in ref 20. To directly compare this model with the spinel models discussed in section 3.2, Figure 4 displays the model containing four unit cells of the nonspinel model but has been rotated to show the fcc oxygen sublattice in spinel-like orientation. As mentioned in the Introduction, there are 96 interstices between the oxygen ions in the 32 cubic cell; 64 are tetrahedral (8a, 8b, and 48f) and 32 are octahedral (16c and 16d), and cations occupy the l8a and 16d positions in spinel structures.[3] In this nonspinel structure, the oxygen sublattice is essentially the same as that of spinel structures, with the key difference being that the cations occupy interstices other than the 18a and 16d positions.

Figure 5 compares the cation positions in the nonspinel structure (A) and the spinel structure (B). In the nonspinel structure, most of tetrahedral aluminum atoms are placed at the 48f positions and some at the 8b positions. Octahedral aluminum atoms are distributed between the 16c and 16d positions, as indicated in Figure 5A. In the spinel structure, cations occupy tetrahedral 8a and octahedral 16d (Figure 5B). The total energy of the nonspinel structure is between the lowest energy structure of anhydrous defect spinel model ($\square^{O}{}_2Al^{T}{}_6Al^{O}{}_{10}O_{24}$) and the structure with the lowest R_p value ($\square^{O}\square^{T}Al^{T}{}_5Al^{O}{}_{11}O_{24}$), with only a 0.07 eV/$Al_2O_3$ difference to either of them (Table 2). Thus, energetically, one cannot distinguish between the nonspinel and spinel structures.

To further compare the nonspinel model with the spinel-related models, the nonspinel model using the structural parameters reported in ref 20 was constructed and analyzed against the experimental SXPD pattern. Figure 6 shows the unrefined Reflex powder diffraction patterns of the four γ-Al_2O_3 models, fully hydrogenated ($H^{T}{}_2H^{O}{}_2Al^{T}{}_6Al^{O}{}_{14}O_{32}$), partly hydrogenated ($H^{O}\square^{T}{}_2Al^{T}{}_6Al^{O}{}_{15}O_{32}$), and fully dehydrogenated ($\square^{O}\square^{T}Al^{T}{}_5Al^{O}{}_{11}O_{24}$) defect spinel-structures and the nonspinel structure, each superimposed with the experimental SXPD pattern. In the analysis of the unrefined simulated diffraction patterns, emphasis is placed on the diffraction angles rather than the profile of the peaks. For the three models that are derived from the spinel structure, there are corresponding diffraction lines at 2θ where major peaks are observed on the experimental SXPD patterns. However, for the nonspinel model, there are no diffraction lines between $2\theta = 13.8$ and 14.8°, whereas a sharp peak at $2\theta = 14.7°$ with a shoulder peak at 14.1° has been recorded. Interestingly, a strong diffraction intensity is observed at $2\theta = 14.4°$ for all the spinel-related models, which are between the two experimental peaks corresponding to tetrahedral aluminum at the 8a positions. Furthermore, the

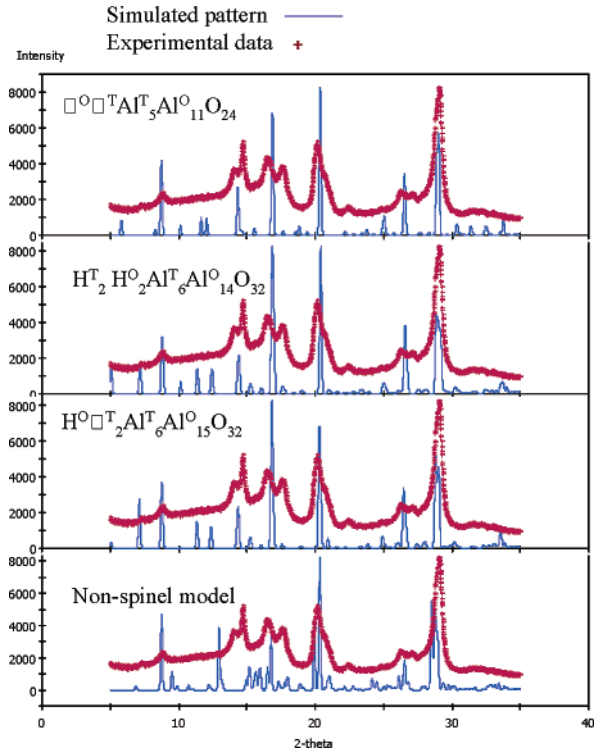

Figure 6. Unrefined simulated powder diffraction patterns of different models in comparison with the experimental SXPD pattern.

diffraction line at approximately $2\theta = 29°$ for the nonspinel model is at a considerably lower angle than the corresponding peak in the SXPD pattern. The simulated diffraction patterns were then optimized using Rietveld refinements only modifying the particle size of the sample without changing lattice parameters of the γ-Al_2O_3. The refined diffraction patterns for the four models are presented in Figure 7 against the experimental SXPD pattern. Following Reitveld refinement, it is clear that the simulated pattern for the nonspinel structural model is completely out of phase with the experimentally observed SXPD pattern at 2θ between 13° and 19°, while the simulated patterns for the spinel-related models match the major peak positions reasonably well. This nonspinel structure has a relatively large R_p value in comparison to the spinel-type models ($\square^{O}\square^{T}Al^{T}{}_5Al^{O}{}_{11}O_{24}$) with vacancies distributed between the tetrahedral and octahedral positions (13.6 vs 10.0%, Table 2). These results strongly suggest that the spinel-related models can represent the details of the γ-Al_2O_3 structure better than the nonspinel model.

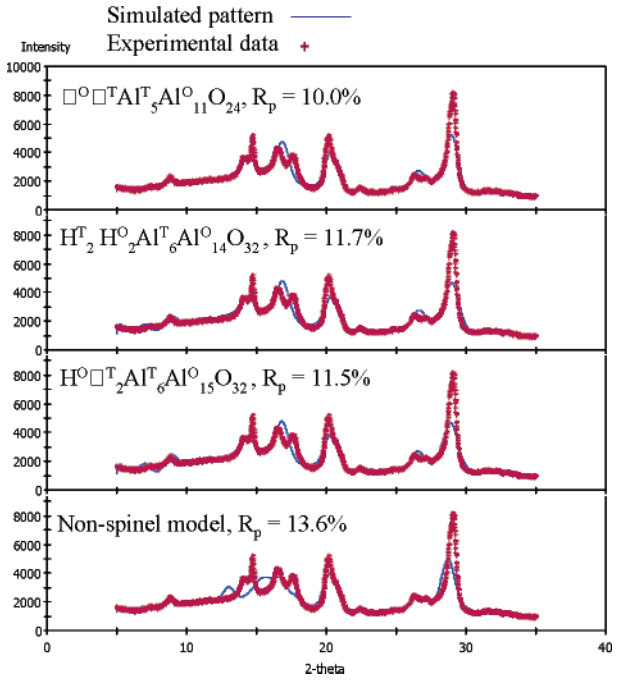

Figure 7. Rietveld-refined powder diffraction patterns of different models in comparison with the experimental SXPD pattern.

TABLE 4: Rietveld Refinement Results for the Spinel-Related Model against Experimental Results from the Literature

properties		simulated values	experimental values
lattice parameters	*a*, Å	8.01 ± 0.03	7.96 (ref 7)
	b, Å	8.01 ± 0.02	7.96
	c, Å	7.81 ± 0.01	7.81
	α	90.1 ± 0.3°	90°
	β	90.1 ± 0.3°	90°
	γ	91.7 ± 0.1°	90°
tetrahedral aluminum		28%	21, 25, 30% (refs 8, 11, 21)
particle size, Å	*A*	80 ± 27	80−90 (ref 15)
	B	87 ± 26	
	C	36 ± 4	
R_p		8.4%	

Another approach to generating a γ-Al_2O_3 model based on a defect spinel structure is to refine a trial structure against an experimental SXPD pattern. As discussed previously, the spinel structure is a reasonably accurate model to describe the structural features of γ-Al_2O_3 compared to the nonspinel structure. Therefore, an additional spinel-related structure was constructed by replacing all magnesium atoms by aluminum from the $MgAl_2O_4$ cubic cell. First, the lattice parameters and the occupancies of aluminum atoms were refined against the experimental SXPD pattern, and then the sample size effect was taken into account. Table 4 presents the structural parameters in comparison with experimental values for this optimized structural model. There is excellent agreement between the simulated and experimental diffraction patterns with respect to the lattice parameters with a corresponding R_p value of only 8.4%. The resulting model predicts a tetragonal cell with a *c*/*a* ratio of about 0.98 ($a = b = 8.01$, $c = 7.81$ Å), which accurately reproduces the experimental observation ($a = b = 7.96$, $c = 7.81$ Å).[7] On the other hand, the nonspinel structure predicts a *c*/*a* ratio of 1.02 ($a = 7.90$, $b = 7.93$, $c = 8.07$) for cell parameters, which does not agree with the experimental data.[20]

Figure 8 displays the simulated and experimental SXPD patterns and the relative difference in diffraction intensities. The agreement between the simulated and the experimental patterns

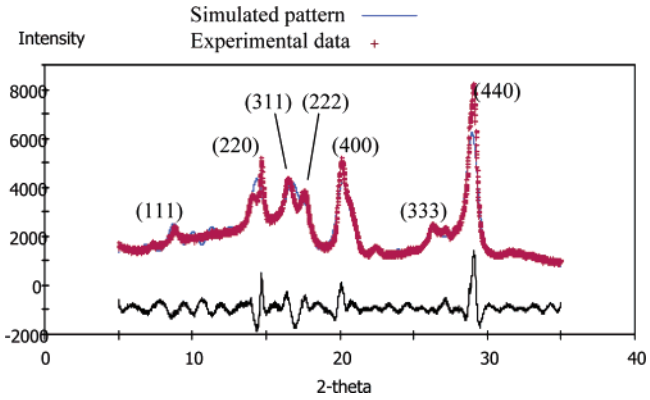

Figure 8. Simulated diffraction pattern of a Rietveld-refined spinel-related model against the experimental SXPD data (X-ray $\lambda = 0.69876$ Å). The solid line at the bottom is the difference between simulated and experimental data.

are much better than that shown in Figure 7 due to the additional refinement of the model structure. The largest discrepancy between the simulated and experimental patterns is at 2θ, around 14.5°, which is due to the (220) reflection. According to Lippens and de Boer[29] and Zhou and Snyder,[13] the (220) reflection represents planes with aluminum in tetrahedral positions. The splitting of the (220) reflection peak indicates that the tetrahedral aluminum cations are highly disordered. None of the models discussed above could reproduce this splitting feature; however, the spinel-related models could accurately predict a reflection that represents the average of the split peaks. The octahedral aluminum is also disordered from perfect spinel positions but to a lesser extent than the tetrahedral sublattice.[13,30] The disordering of aluminum cations in γ-Al_2O_3 makes it impossible to obtain an accurate model to represent all the detailed structural features with a simple model.[6,30,31] However, the spinel-related model can represent major features of γ-Al_2O_3 reasonably well, which can be used in future theoretical studies of surface properties and modification by elemental doping and incorporation.

4. Conclusions

Combining DFT calculations and Rietveld refinement simulations, three spinel-related models for γ-Al_2O_3 which contain different amounts of hydrogen in the bulk structure were evaluated and further compared with a nonspinel model that was built based on molecular dynamic simulation and DFT calculations of the dehydration of boehmite.[19,20] For spinel-related models, the fully hydrogenated structure is energetically more stable than anhydrous defect spinel structures below 550 K. The simulated X-ray powder diffraction pattern of the anhydrous defect spinel structure is in better agreement with the experimental SXPD pattern. For fully hydrogenated spinel-related models, hydrogen forms bulk hydroxyl groups at both tetrahedral and octahedral sites. For partly hydrogenated models, hydrogen and vacancies tend to distribute at different types of sites; when hydrogen forms hydroxyl groups at octahedral sites and vacancies are located at tetrahedral sites, the simulated diffraction pattern is in excellent agreement with the experimental SXPD pattern. For fully dehydrogenated defect spinel models, cation vacancies are energetically preferred at octahedral sites but the structure with vacancies distributed between the two types of sites has the best fit with experimental data. All three types of spinel-related models have a smaller error than the nonspinel model when compared to the experimental SXPD pattern. The nonspinel model cannot reproduce the SXPD

reflection originating from the tetrahedral aluminum plane in the (220) direction. The Rietveld-refined spinel model can accurately produce the lattice parameters and the correct ratio of tetrahedral to octahedral aluminum. Therefore, the spinel-related structure model is better than the nonspinel model in description of the bulk structure of γ-Al_2O_3.

Acknowledgment. The authors thank Peter Stephens at the State University of New York, Stony Brook, for technical assistance and the collection of the SXPD pattern. This work is supported by Syncrude Canada Ltd. and the Natural Sciences and Engineering Research Council (NSERC) under Grant No. CRDPJ 261129. Research was carried out (in whole or in part) at the National Synchrotron Light Source, Brookhaven National Laboratory, which is supported by the U.S. Department of Energy, Division of Materials Sciences and Division of Chemical Sciences, under Contract No. DE-AC02-98CH10886.

References and Notes

(1) Poisson, R.; Brunelle, J.-P.; Nortier, P. In *Alumina, Catalysts supports and Catalysts*; Stiles, A. B., Eds.; Butterworth: Boston, MA, 1987.
(2) Ertl, G.; Knözinger, H.; Weitkamp J. *The Handbook of Heterogeneous Catalysis*; Wiley-VCH: Weinheim, Germany, 1997.
(3) Wyckoff, R. W. G. *Crystal Structures*; Interscience Publishers: New York, 1963; Vol. 3, p 76.
(4) Chou, T. C.; Nieh, T. G. *J. Am. Ceram. Soc*. **1991**, *74*, 2270−2279.
(5) Sickafus, K. E.; Wills, J. M.; Grimes, N. W. *J. Am. Ceram. Soc*. **1999**, *82*, 3279−3292.
(6) Wolverton, C.; Hass, K. C. *Phys. Rev. B* **2000**, *63*, 24102-1−16.
(7) Wilson, S. J. *J. Solid State Chem*. **1979**, *30*, 247−255.
(8) Lee, M.-H.; Cheng C.-F.; Heine, V.; Klinowski, J. *Chem. Phys. Lett.* **1997**, *265*, 673−676.
(9) Wang, J. A.; Bokhimi, X.; Morales, A.; Novaro O.; López, T.; Gómez, R. *J. Phys. Chem. B* **1999**, *103*, 299.
(10) Jayaram, V.; Levi, C. G. *Acta Metall*. **1989**, *37*, 569−578.
(11) Pecharromán, C.; Sobrados, I.; Iglesias, J. E.; González-Carreño, T.; Sanz, J. *J. Phys. Chem. B* **1999**, *103*, 6160−6170.
(12) Sohlberg, K.; Pennycook, S. J.; Pantelides, S. T. *J. Am. Chem. Soc.* **1999**, *121*, 7493−7499.
(13) Zhou, R. S.; Snyder, R. L. *Acta Crystallogr., Sect. B*: *Struct. Sci.* **1991**, *47*, 617−630.
(14) Pearson, R. M. *J. Catal*. **1971**, *23*, 388−394.
(15) Soled, S. *J. Catal.* **1983**, *81*, 252−257.
(16) Tsyganenko, A. A.; Smirnov, K. S.; Rzhevskij, A. M.; Mardilovich, P. P. *Mater. Chem. Phys*. **1990**, *26*, 35−46.
(17) Paglia, G.; Buckley, C. E.; Udovic, T. J.; Rohl, A. L.; Jones, F.; Maitland, C. F.; Connolly, J. *Chem. Mater*. **2004**, *16*, 1914−1923.
(18) Ushakov, V. A.; Moroz, E. M. *React. Kinet. Catal. Lett*. **1984**, *24*, 113−118.
(19) Krokidis, X.; Raybaud, P.; Gobichon, A. E.; Rebours, B.; Euzen, P.; Toulhoat, H. *J. Phys. Chem B* **2001**, *105*, 5121−5130.
(20) Digne, M.; Sautet, P.; Raybaud, P.; Euzen, P.; Toulhoat, H. *J. Catal.* **2004**, *226*, 54−68.
(21) John, C. S.; Alma, N. C. M.; Hays, G. R. *Appl. Catal*. **1983**, *6*, 341−346.
(22) Segall, M. D.; Lindan, P. J. D.; Probert, M. J.; Pickard, C. J.; Hasnip, P. J.; Clark, S. J.; Payne, M. C. *J. Phys.: Condens. Matter* **2002**, *14*, 2717−2744.
(23) Vanderbilt, D. *Phys. Rev. B* **1990**, *41*, 7892−7895.
(24) Perdew, J. P.; Burke, K.; Ernzerhof, M. *Phys. Rev. Lett*. **1996**, *77*, 3865−3868.
(25) Rietveld, H. M. *J. Appl. Crystallogr*. **1969**, *2*, 65−71.
(26) Young, R. A. *The Rietveld Method*, *IUCr Monographies of Crystallography 5*; Oxford University Press: Oxford, U.K., 1993.
(27) Wyckoff, R. W. G. *Crystal Structures*; Interscience Publishers: New York, 1963; Vol. 2, p 7.
(28) http://webbook.nist.gov/chemistry/.
(29) Lippens, B. C.; de Boer, J. H. *Acta Crystallogr*. **1964**, *17*, 1312−1321.
(30) Paglia, G.; Buckley, C. E.; Rohl, A. L.; Hart, R. D.; Winter, K.; Studer, A. J.; Hunter, B. A.; Hanna, J. V. *Chem. Mater*. **2004**, *16*, 220−236.
(31) Paglia, G.; Buckley, C. E.; Rohl, A. L.; Hunter, B. A.; Hart, R. D.; Hanna, J. V.; Byrne, L. T. *Phys. Rev. B* **2003**, *68*, 144110-1−11.